



**Titre:** Processing parameters investigation for the fabrication of self-supported and freeform polymeric microstructures using ultraviolet-assisted three-dimensional printing  
**Title:**

**Auteurs:** Rouhollah Dermanaki Farahani, Louis Laberge Lebel, & Daniel Therriault  
**Authors:**

**Date:** 2014

**Type:** Article de revue / Article


**Référence:** Farahani, R. D., Laberge Lebel, L., & Therriault, D. (2014). Processing parameters investigation for the fabrication of self-supported and freeform polymeric microstructures using ultraviolet-assisted three-dimensional printing. Journal of Micromechanics and Microengineering, 24(5), 055020 (12 pages).  
**Citation:** <https://doi.org/10.1088/0960-1317/24/5/055020>

 **Document en libre accès dans PolyPublie**  
Open Access document in PolyPublie

**URL de PolyPublie:** <https://publications.polymtl.ca/10406/>  
**PolyPublie URL:**

**Version:** Version finale avant publication / Accepted version  
Révisé par les pairs / Refereed

**Conditions d'utilisation:** Tous droits réservés / All rights reserved  
**Terms of Use:**

 **Document publié chez l'éditeur officiel**  
Document issued by the official publisher

**Titre de la revue:** Journal of Micromechanics and Microengineering (vol. 24, no. 5)  
**Journal Title:**

**Maison d'édition:** IOP Publishing Ltd  
**Publisher:**

**URL officiel:** <https://doi.org/10.1088/0960-1317/24/5/055020>  
**Official URL:**

**Mention légale:** ©2014. This is the author's version of an article that appeared in Journal of Micromechanics and Microengineering (vol. 24, no. 5) . The final published version is available at <https://doi.org/10.1088/0960-1317/24/5/055020>  
**Legal notice:**

# Processing Parameters Investigation for the Fabrication of Self-supported and Freeform Polymeric Microstructures Using Ultraviolet-Assisted Threedimensional Printing

R D Farahani, L L Lebel, and D Therriault

Laboratory for Multiscale Mechanics, Center for Applied Research on Polymers (CREPEC)  
École Polytechnique de Montréal, P. 6079, succ. Centre-Ville, Montreal, H3C 3A7 Canada

\* Corresponding author:

Phone: 514-340-4711 x449; Fax: 514-340-4176;

E-mail: daniel.therriault@polymtl.ca

**Abstract** The ultraviolet-assisted 3D printing (UV3DP) was used to manufacture photopolymer-based microdevices with self-supported and freeform features. The UV3DP technique consists of the robotized deposition of extruded filaments, which are rapidly photopolymerized under UV illumination during the deposition process. This paper systematically studies the processing parameters of the UV3DP technique using two photocurable polymers and their associated nanocomposite materials. The main processing parameters including materials' rheological behavior, deposition speed and extrusion pressure, and UV illumination conditions were thoroughly investigated. A processing map was then defined in order to help choosing the proper parameters for the UV3D printing of microstructures with various geometries. Compared to self-supported features, the accurate fabrication of 3D freeform structures was found to take place in a narrower processing region since a higher rigidity of the extruded filament was required for structural stability. Finally, various 3D self-supported and freeform microstructures with high potential in micro electromechanical systems, microsystems and organic electronics were fabricated to show the capability of the technique.

Submitted to Journal of Micromechanics and Microengineering

## 1. Introduction

Micro- and nanotechnological systems using photopolymers and their associated nanocomposite materials have gained considerable attention in various fields such as micro electromechanical systems (MEMS) [1], microelectronics [2], optoelectronics [3], biotechnology [4] and microchemical systems [5]. Despite the wide variety of applications, device miniaturization and threedimensional (3D) shape optimization have not reached their full potential, partly due to the lack of easy and cost-effective manufacturing techniques. Standard microfabrication techniques such as stereolithographic techniques [6,7] have been adapted to fabricate 3D products using photopolymers. Ultraviolet-assisted 3D-printing (UV-3DP) [8] is an alternative technique to manufacture photopolymer-based microdevices with self-supported or supported features. Figure 1 is a

schematic of the UV-3DP fabrication of a freeform helical microspring. This technique relies on the robotically-controlled microextrusion of a UV-curable ink filament through a capillary nozzle while the extrusion point is moved in three directions. The uncured ink material is photopolymerized within seconds after extrusion under UV illumination that moves along the extrusion point. Upon curing, the increased rigidity of the extruded filament enables the creation of multidirectional shapes (3D freeform and self-supported) layout along the trajectory of the extrusion point. Compared to conventional microfabrication techniques, the UV-3DP exhibits a high level of flexibility, cost effectiveness and fabrication rate.

Despite the flexibility of the UV-3DP technique, the type of UV-curable materials as well as the processing parameters have to be carefully adjusted to build a precise 3D microstructure. In this paper, we systematically investigate all the main processing parameters such as deposition speed (i.e., extrusion point moving speed), extrusion pressure, material viscosity, and UV-exposure region. The influence of each parameter was studied for the fabrication of 3D self-supported and freeform microstructures using the UV-3D printing of UV-curable thermosetting resins and their associated nanocomposite materials. One of the main outcomes of this investigation is the creation of a processing map which can be used as a guide for the fabrication of different 3D geometries.

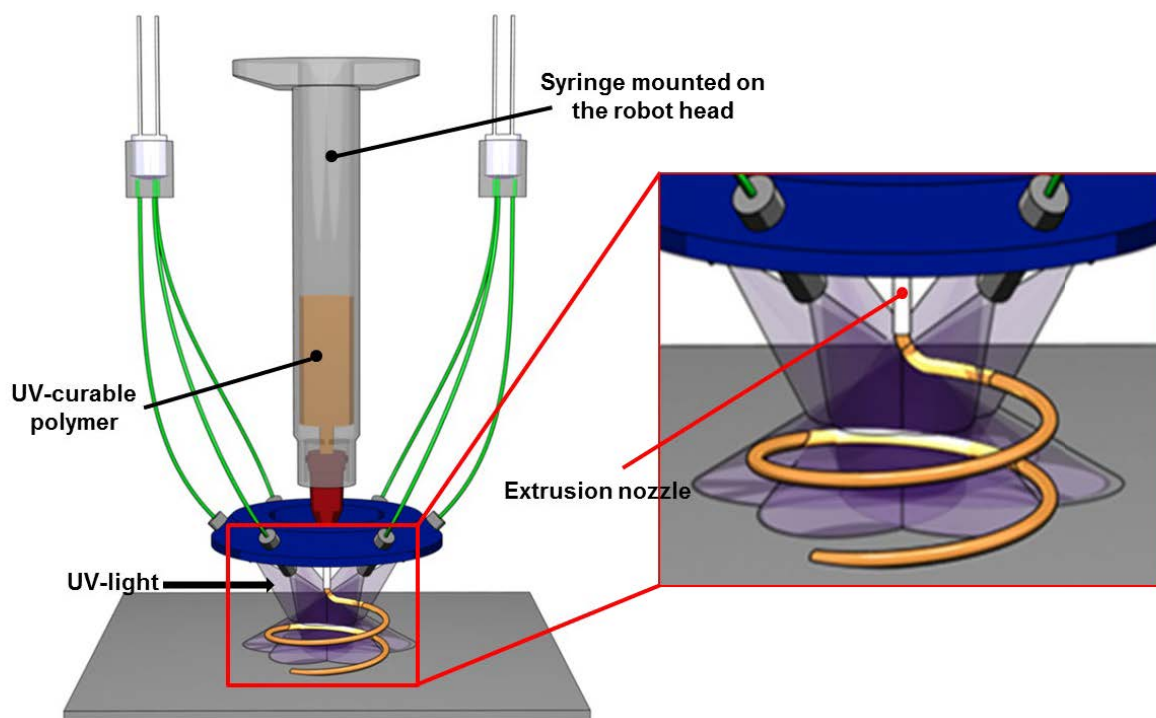


Figure 1. A scheme of the UV-assisted fabrication of a microspring made of a photopolymer. The material is extruded through a micronozzle and is rapidly photopolymerized under the UV illumination provided by a set of optical fibers.

## 2. Experimental Details

### 2.1. Materials

The materials used as the ink materials in this study were commercially available one component dual cure resins (UV/heat curable) resins which were used either as they were received or after being rheologically modified (e.g., mixing with nanoparticles). The resins were either polyurethane based (NEA123MB & NEA123T, Norland Products) or epoxy based (UV15DC80, Master Bond Inc.) materials. The resins contained UV photo-initiators having a maximum absorption at 365 nm and a heater active in the 60–80 °C range. Nanoparticles such as fumed silica (Aerosil 200, Degussa) and single-walled carbon nanotubes [9] were added to the resins to make nanocomposite inks. These nanocomposite ink materials were prepared by blending the resins and the nanofillers using ultrasonication and the ball mill mixing methods (more details on the nanocomposite inks preparation can be found elsewhere [8–10]). The inks were stored in UV protective 3CC syringes (Nordson EFD) at room temperature. Based on our experience, the materials remain stable at least for a year under the above conditions.

### 2.2. UV-3DP Experimental Setup

Figure 2 shows images of the UV-3DP setup and deposition of a microspring using this technique. The UV direct-writing platform is composed of a computer-controlled robot (I & J2204, I & J Fisnar) that moves a dispensing apparatus (KFEFD) and a UV light emission setup along the x, y and z axes using a commercial software (JR Points for Dispensing, Janome Sewing Machine). The dispensing apparatus mounted on the robot head carries a 3 CC syringe (Nordson EFD) of the ink material (Figure 2a) which is then extruded by an applied pressure. This apparatus is connected to a pneumatic fluid dispenser (Ultra™ 2400 series, EFD) which can provide extrusion pressure up to 4.9 MPa. The UV light is provided by two high intensity UV light-emitting diodes (LED, NCSU033A, Nichia) having a wavelength centered at 365. A set of six optical fibers arranged in a circular pattern (Figure 2c) deliver the UV light close to the tip of the extrusion micronozzle (Precision Stainless Steel Tips, EFD). The intensity of the present UV radiation is  $50 \text{ W cm}^{-2}$  measured using a UV intensity probe (UV Intensity meter, model 100, Karl Suss). [The fast curing of the ink enables the fabrication of self-supported and freeform 3D structures when the extrusion position spatially changes (Figure 2d)]

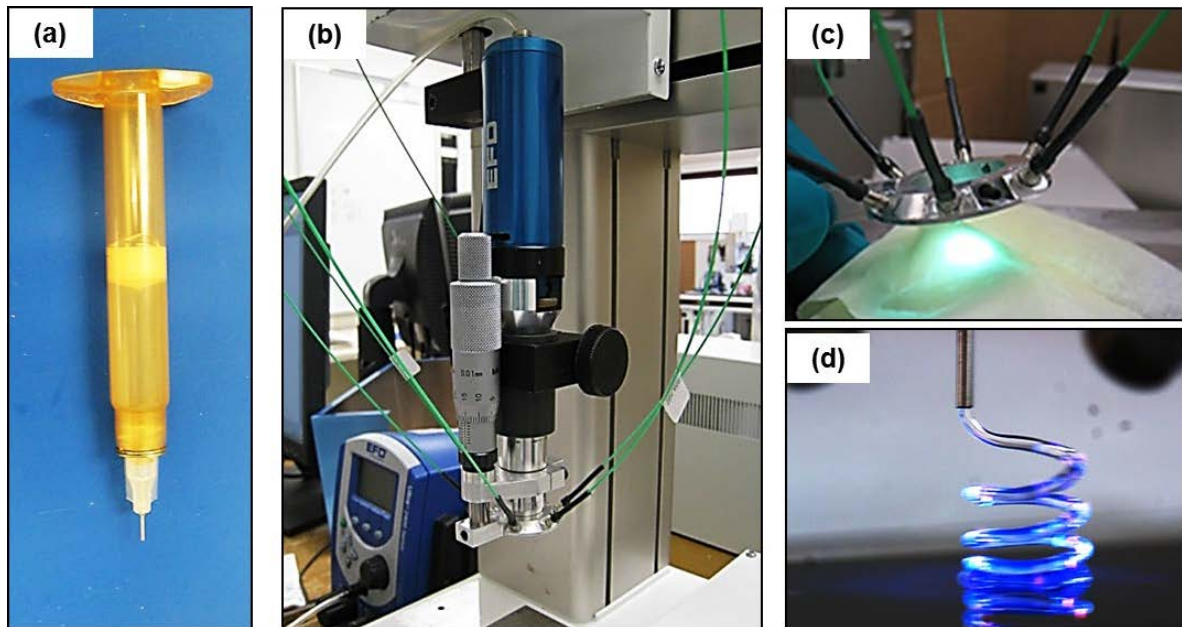


Figure 2.(a) a 3 CC syringe containing UV-curable material (b) the deposition setup with inserted syringe and pressure piston mounted on the computer-controlled robot (c) UV light delivery system consisting of six fiber optics showing UV radiation emitted from the robot in (b), and (d) image of a microspring deposition using a UV-curable ink

### 2.3. UV-3DP Fabrication of 3D self-supported and freeform microstructures

Stainless steel micro nozzles with two different internal diameters ( $D$  of 100  $\mu\text{m}$  and 150  $\mu\text{m}$ ) were used with 3 CC syringes. As a self-supported structure, a 3D periodic scaffold was fabricated which has potential applications in tissue engineering [10]. The fabrication of the scaffold began with the deposition of the ink filaments on a substrate, leading to a 2D pattern. After following layers were deposited by successively incrementing the position of the dispensing nozzle by the diameter of the filaments and changing the dispensing direction by 90° rotation from the underlying layer. The fabricated scaffold consisted of several layers (e.g., 4 layers) of the ink filaments in which each layer was alternatively oriented perpendicular to or along the first deposited layer. This process was repeated until the desired 3D scaffold was created.

3D freeform microstructures featuring different geometries were also manufactured using the UV-3DP technique. The first fabricated microdevice was composed of a set of freeform vertical filaments having a diameter of  $\sim 50 \mu\text{m}$  in a square layout of  $4 \times 4$  micro rods. Networks of 3D helical microstructures composed of up to 15 microsprings were also accurately manufactured.

### 2.4. Ink viscosity characterization

An experimental method based on capillary viscometry [10, 12] was used to measure the process-related apparent viscosity of the ink. To obtain different shear conditions, ten continuous filaments of material were extruded through a micro nozzle (510-0.25-B, Precision Stainless Steel Tips, EFD, length of  $\sim 16\text{mm}$  and internal diameter of 150  $\mu\text{m}$ ) at same pressure over a glass substrate

and was repeated five different pressures (i.e., 0.7, 1.4, 2.1, 2.8, and 3.5 MPa). The filaments were deposited using the dispensing robot with a calibrated deposition speed. Shortly after the deposition, the filaments were cured under a UV lamp (97600, ColeParmer) illumination for 5 min. The material flow rate during the extrusion was calculated by multiplying the deposition speed by the deposited filaments cross-section. The cross-section area of the filaments was measured with an optical microscope (BX61, Olympus) and image analysis software (Image Plus V6, Media Cybernetics). The possible error for the calculation of filament cross-section area upon curing was negligible since the materials shrinkage is < 1% according to the supplier process. The apparent viscosity and the process-related shear rate were calculated from capillary viscometry equations including Rabinowitsch correction [10,12]. The end effects called Bagley correction are negligible in the viscosity calculations because of the very high capillary aspect ratio (i.e., length/diameter of the extrusion nozzle used  $L/D \sim 106$ ).

## 2.5. Morphological characterization of fabricated microstructures

The structures fabricated through different processing conditions were observed using an optical microscope (BX61, Olympus) and image analysis software (Image Plus V7, Media Cybernetics) in order to find the processing map for a successful UV direct writing. The morphology of the representative self-supported and freeform microstructures was also observed either by optical microscopy or field emission scanning electron microscopy (FESEM JEOL, 7600 FFE).

## 3. Results and discussion

### 3.1. Material properties

The materials viscosity is probably the most important parameter of the direct write techniques. Materials with moderate to high viscosities are necessary to extrude stable filaments [13,14]. Since the high viscosity may limit flow through fine extrusion nozzles, an extruded material's shear thinning behavior (i.e., a decrease of viscosity with an increase of shear rate inside the nozzle) is preferable. For shear thinning inks, their rigidity increases when exiting the extrusion nozzle, that is, when the shear strain applied to the material returns to a near zero value. This rigidity allows the filaments shape retention and enables to fabricate self-supported 3D structures. However to fabricate freeform 3D structures, a further increase of rigidity is required that is provided by the polymerization of the inks in the UVDP technique [8].

Figure 3 shows the process-related apparent viscosity ( $\eta_{app}$ ) with respect to the process-related shear rates ( $\dot{\gamma}$ ) obtained using our capillary viscometry technique for all the materials used in this study. Figure 3a shows the viscometry results for the UV-curable urethane-based (UVPU) materials. A nearly constant  $\eta_{app}$  of  $\sim 6$  Pa.s was observed for the pure NEA123MB, indicating a Newtonian behavior in the range of shear rates studied. The incorporation of 5 wt% si

nanoparticles into this pure resin resulted in a considerable increase of  $\eta_{0.6}$  at low  $\dot{\gamma}$  and also a shear thinning rheological behavior. This increase might be due to a weak network formation of hydrogen bonded fumed silica particles which caused a gel-like rheological behavior to the mixture at rest. The weakly bounded network is then destroyed under moderate shear forcing is the reduction of the viscosity. The second type of UPU (NEA 123T) which was used as received (contains nanoparticles which were already added by the supplier) shows a relatively high viscosity and a shear thinning behavior without further adding nanofillers (Figure 3a). Figure 3b shows the results obtained for the viscosity of UV-curable epoxy based (UV-epoxy) materials. Similar to the pure NEA123MB, a Newtonian behavior was observed for the viscosity of the UV-epoxy resin with a slightly higher value of  $\sim 17$  Pa.s. The  $\eta_{0.6}$  of the resin increased by the addition of 0.5 wt% of CNTs. Further increases of the viscosity were achieved with the increase of CNTs concentrations (1wt% and 2wt%). A shear thinning behavior of the resulting nanocomposites with different power indices (slope of the curves) was also observed. The carbon nanotubes high aspect ratio possibly enabled the formation of a rheological percolation network and also their possible orientation during extrusion are thought to be responsible for the observed shear thinning behavior.

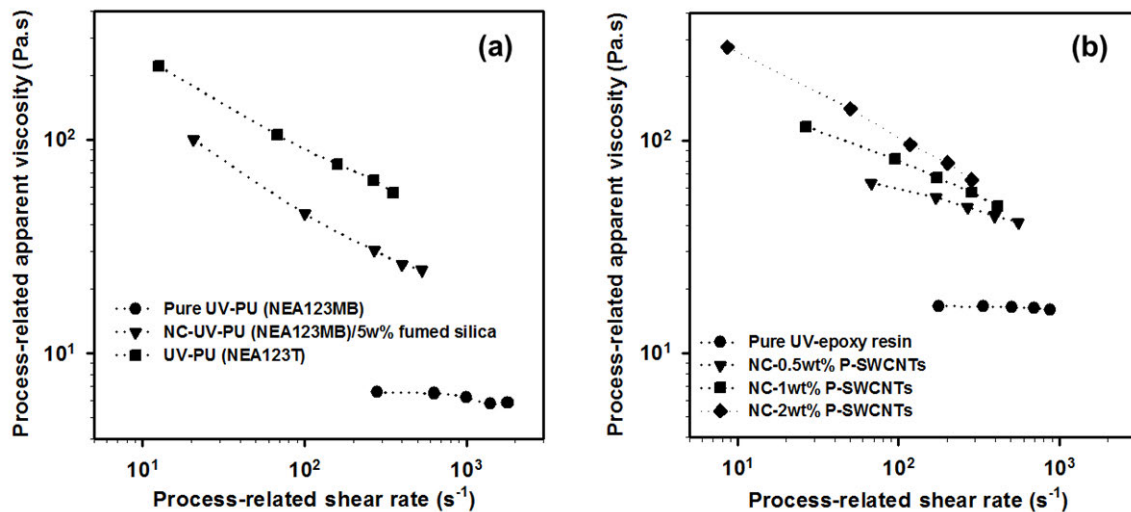


Figure 3. Process-related apparent viscosity of the ink materials with respect to process-related shear rate using a method based on capillary viscometry: (a) UVPU resins and (b) UV-curable epoxy based resin and its associated CNT reinforced nanocomposites.

Figure 4 shows the effect of viscosity (or rheological behavior) of the representative materials used in this study on the UV3DP fabrication of freeform microsprings. Figure 4a shows an unsuccessful fabrication of the designed microspring when the viscosity Newtonian UPU (pure NEA123MB) was used. As it can be seen in the inset of Figure 4a, the viscosity of the material used seems not to be high enough to create a stable filament. Similar behavior was also observed for low-viscosity Newtonian pure UV-epoxy (the result is not shown). However, the fabrication of microsprings was successful when the materials with higher viscosities were used. Figure 4b shows a



representative optical image of a fabricated microspring with 7 coils using VPU (NEA 123T) and a stable filament is observed in the inset image. Similarly, a microspring with 6 coils was fabricated using the UV-epoxy containing 1wt.% CNTs as a result of its relatively high viscosity, as shown in Figure 4c. The higher viscosity prevents sagging of the extruded filament prior to curing under UV exposure, as filamentary shape is observed for both materials in the inset of the figures.

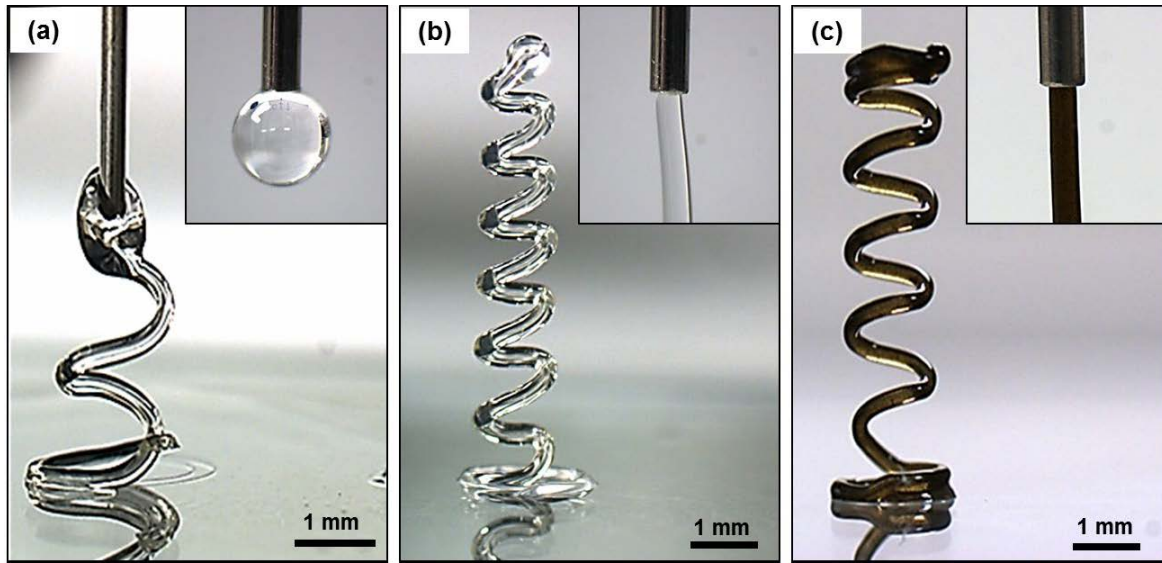


Figure 4. Optical images of UV-3DP fabrication of microsprings using three representative materials (a) the pure NEA 123MB (low viscosity material), and (b) and (c) NEA 123T and the epoxy containing 1wt.% CNTs (high viscosity materials). The images show the viscosity-dependent stability of filaments to build a structure with desired shape, in this case, a microspring.

In case of the pure low viscosity resins, the addition of nanofillers was a key in order to increase the resins viscosity and make them suitable for successful UV-3D printing while the observed sheath thinning behavior facilitated materials extrusion at lower pressures. However, the addition of higher loadings especially in case of CNTs may decrease the resins transparency and consequently their photopolymerization rates, and thus, lowers the fabrication rate.

### 3.2. Processing criteria

Material conversion rate (the ratio of the material conversion from 0 for the uncured viscous liquid to 100% for the completely cured solid) is a crucial parameter for an accurate UV 3D printing. It depends on both the intrinsic properties of the material (e.g., type of monomer, photopolymerization mechanism, etc.) and also processing parameters such as the thickness (or diameter) of the extruded filaments, the intensity of the UV, its distance from the extrusion point and the UV exposure time. For an accurate 3D supported or free fabrication, the photoinitiated polymerization of monomers should occur within seconds to a given degree of



materials conversion  $G H I L Q H G_c$  which is the required increase of rigidity. Figure 5 schematically represents the material process related photopolymerization mechanism during UV-3DP fabrication of a filament. Depending on designed geometries, either self-supported or freeform features, a specific value for  $\alpha_c$  may be required. In particular, to accurately fabricate a 3D freeform microspring, the extruded filament must stay under the exposure for a certain time until it reaches enough rigidity, being able to mechanically support newly liquid extruded material (high  $\alpha_c$  values). This value may be lower for self-supported periodic scaffold or even for the vertical rods. Considering all the parameters, we can come to the conclusion  $\alpha_c$  is influenced by three major processing parameters: radiation exposure length (region), deposition speed and extrusion pressure, which are thoroughly discussed in the following sections. For each parameter, only representative optical images of structures fabricated using an extrusion nozzle of 50  $\mu m$  internal diameter and the UV-PU resin, NEA 123T will be shown. Finally, a processing map will be drawn to show the capability of the UV3DP technique for the fabrication of various microstructures with different geometries.

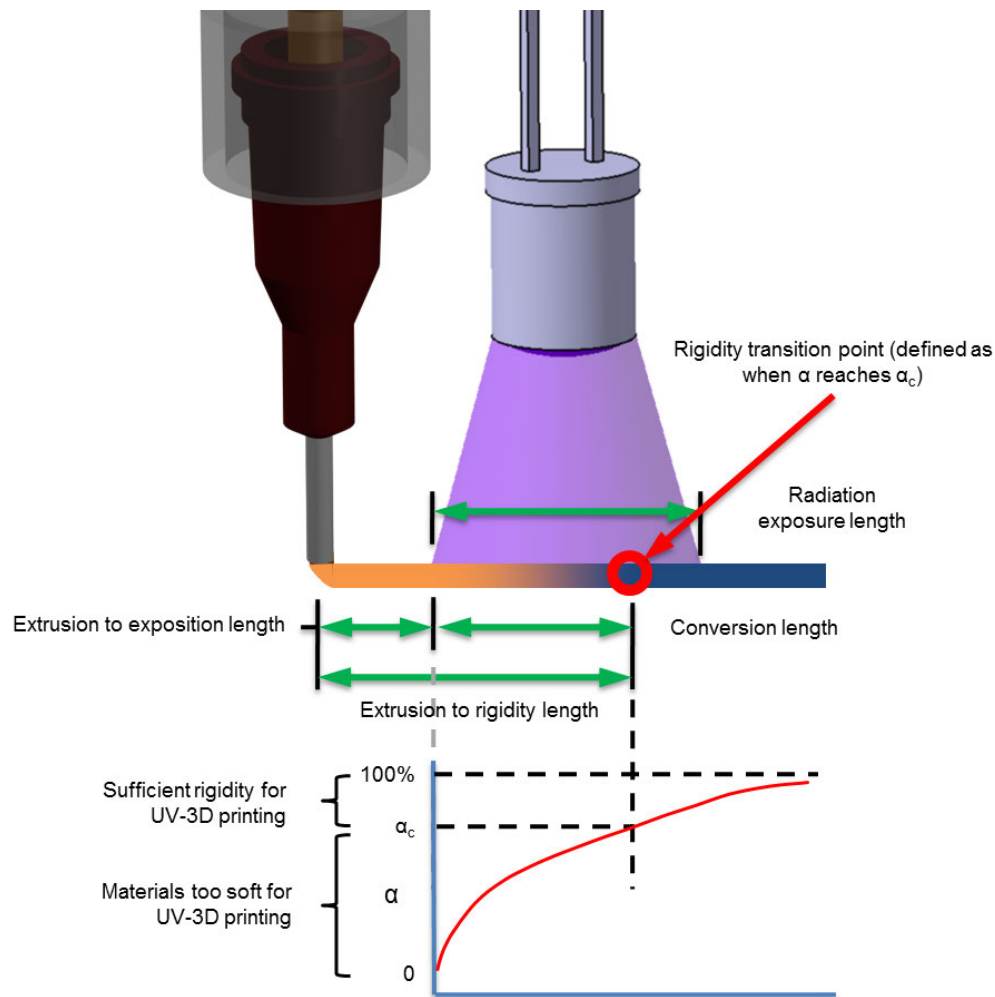


Figure 5. Schematic representation of the material process related photopolymerization mechanism during the UV3DP fabrication of a filament.

### 3.2.1. Radiation exposure length (UV-exposure zone)

The radiation exposure length or UV-exposure zone is shown in Figure 5. This parameter is controlled by moving the UV source (i.e., the rig with six fiber optics shown in Figure 2c) upward and downward. The UV-exposure zone is adjusted such that the filament is exposed to the UV radiation slightly after extrusion (i.e., extrusion to exposition length as shown in Figure 5). This allows the increase in rigidity upon curing to occur away from the extrusion point. However, radiation must nonetheless remain as close as possible to the extrusion point in order to produce the specific path of the moving extrusion device (i.e., short extrusion to exposition length as shown in Figure 5).

Figure 6 shows the effect of radiation exposure length on the fabrication of freeform microsprings. Figure 6a is schematic of a designed microspring (5 coils, coil diameter of 1 mm and filament diameter of 150  $\mu\text{m}$ ) to be fabricated while Figure 6b and 6c shows the optical images of an unsuccessful fabrication resulting from an incorrect positioning of UV radiation apparatus. The material used here was LPU (NEA 123T) and the extrusion nozzle ID was 150  $\mu\text{m}$ . Figure 6b shows the structures fabricated when the tip of extrusion nozzle is in the UV-light (i.e., extrusion to exposition length equals to 0 mm) by which the nozzle might be clogged by cured materials. However, when UV radiation was adjusted far from the extrusion nozzle (i.e., long extrusion to exposition length), the extruded filaments did not reach the desired U L J L G L W < . J) to provide structural support for the material being deposited, resulting in a shape structures (Figure 6c).

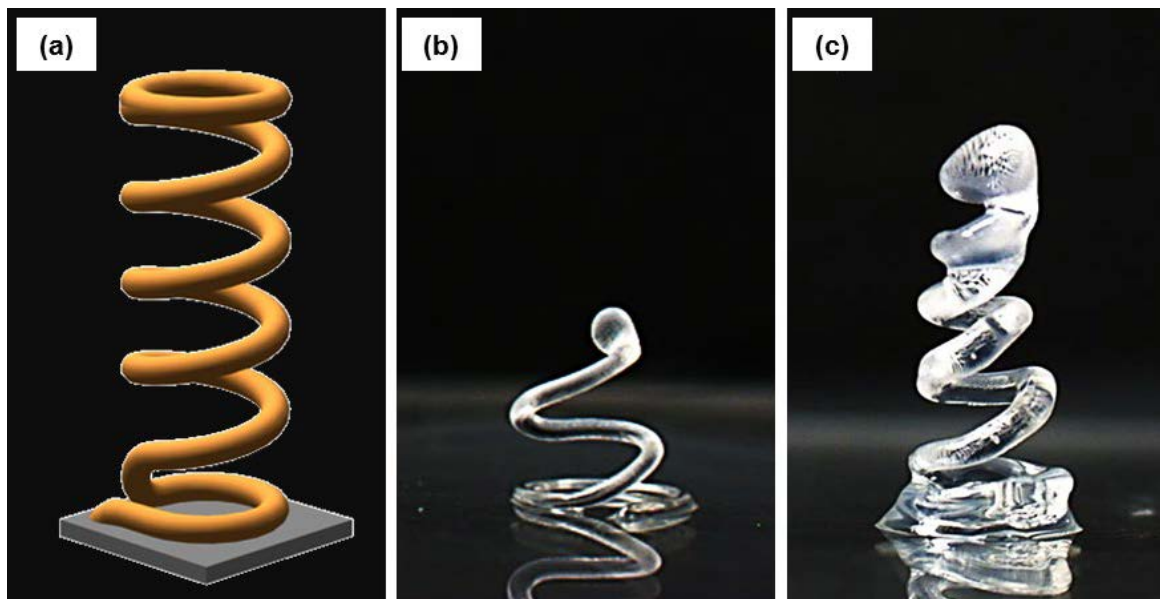


Figure 6. Incorrect adjustment of UV exposure region: (a) virtual image of the programmed path of the extrusion nozzle, (b) the extrusion nozzle is very close to UV exposure region, and (c) the extrusion nozzle is too far from UV-exposure region so the filament meets the UV light later than it has to. The deposition carried out at a deposition speed of 0.3 mm/s and extrusion pressure of  $\sim 1$  MPa using an extrusion nozzle of 150  $\mu\text{m}$  internal diameter and the LPU resin, NEA 123T.

### 3.2.2. Deposition speed

Figure 7 shows optical images of the vertical lines (Fig. 7a) and microsprings (Fig. 7b) fabricated at different deposition speeds (0.1 – 0.7 mm/s) while maintaining a constant extrusion pressure of 4 MPa. In order to better interpret the results, the extrusion speed of the material inside the micronozzle was estimated for the extrusion pressure of 4 MPa. The extrusion speed cannot be controlled directly and is the extrusion pressure dependent. At the extrusion pressure of 1 MPa, the apparent viscosity of material was extrapolated from the viscosity curve of UPU (NEA 123T) shown in Figure 3a. The associated extrusion speed,  $Q_4$ , was then estimated from the following popular capillary equation:

$$Q_4 = \frac{4^6 \Delta p^2}{8 \eta_a \pi R^4 L} \quad (M1)$$

where  $\eta_a$  is the extrapolated apparent viscosity of the material and  $\Delta p$  is the pressure drop,  $R$  and  $L$  are radius and length of the extrusion nozzle, respectively. It should be mentioned that the estimated extrusion speed value might not be accurate and calculated to help better interpretation of the results by comparing the deposition and extrusion speeds. For the extrusion pressure of 4 MPa, extrapolated value of  $\eta_a$  was ~ 115 Pa.s and the extrusion speed was estimated 0.4 mm/s. At the relatively low deposition speeds (0.1 – 0.2 mm/s) the lines were straight and stable having a diameter much larger than the internal needle diameter due to mismatching the deposition speed (< 0.4 mm/s) and the extrusion speed and also swelling of the material after the exit of the extrusion nozzle. The UV-exposure time was enough to allow the complete curing of the filaments (i.e.,  $U \geq R \cdot Q$ ) and thus the fabricated lines were straight. However, a slight instability like waviness of the filaments was observed at the speed of 0.3 mm/s. The filaments' diameter varied depending on the material possible swelling and the deposition speed. As the deposition speed increased, the filaments diameter decreased and the straight filaments were observed. At the deposition speed of 0.4 mm/s, the filament was straight with a diameter close to the ID of the micronozzle, indicating the possible match between the deposition speed and extrusion pressure/speed. At higher speeds (0.6 – 0.7 mm/s) the possible stretching of the extruded material (deposition speed > extrusion speed) also affected the filament diameter. As the deposition speed increased, the length of the vertical filaments reduced and a bubble shape was observed at the top end of the vertical filament. The reason is that the extrusion nozzle moved to the robot origin after it reached the final extrusion point and thus the last extruded materials did not meet the UV light enough to reach the required rigidity. Therefore, the short UV-exposure time (long extrusion to rigidity length) resulted in an incomplete polymerization of materials at the top of filaments (i.e.,  $U < R \cdot Q$ ). This problem can be addressed by keeping the extrusion nozzle at the last extrusion point for a few seconds while no more ink is extruded.

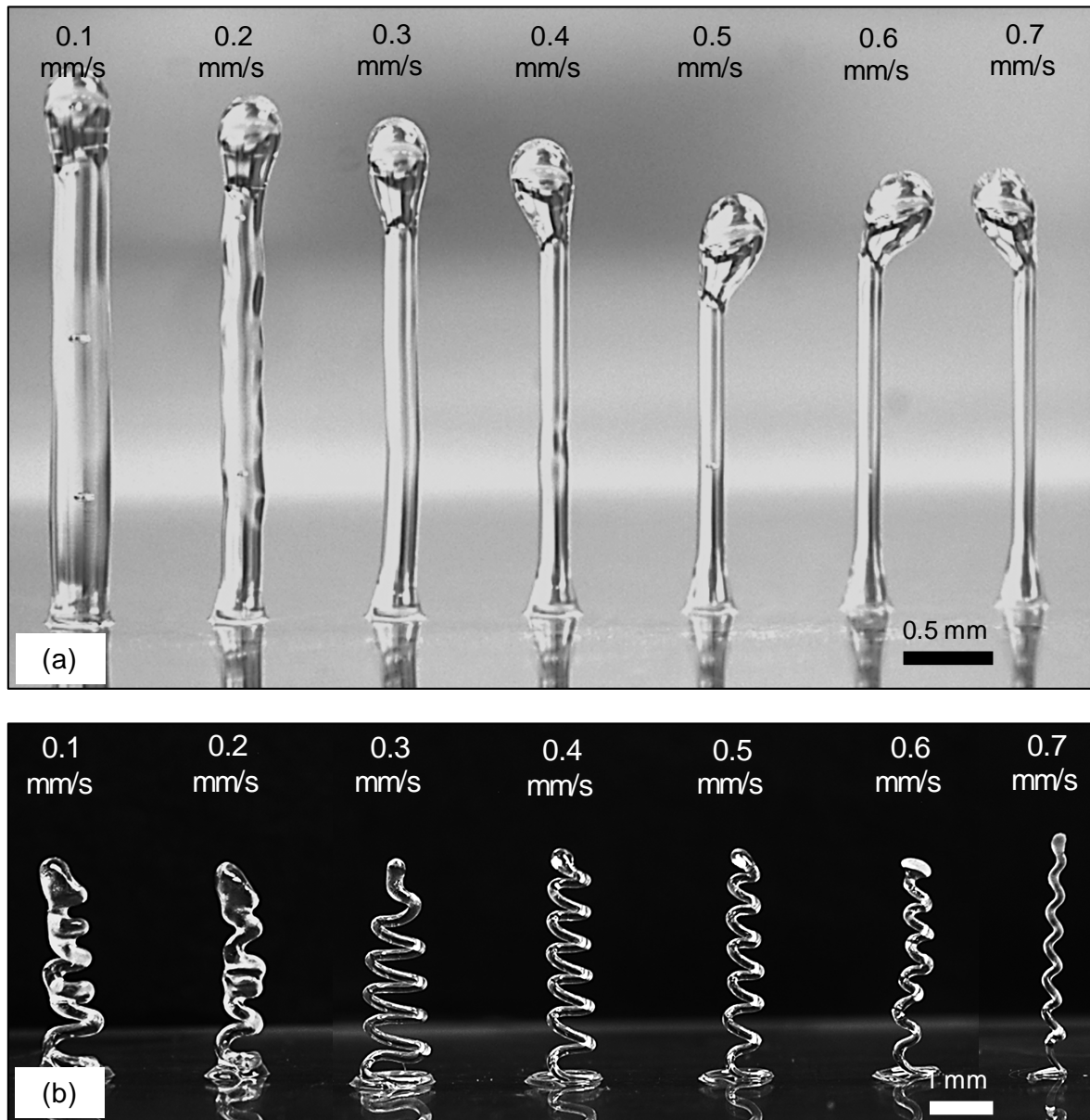


Figure 7. UV-3DP fabrication of (a) vertical filaments and (b) freeform microsprings at different deposition speeds and a constant extrusion pressure of ~ 1 MPa using an extrusion nozzle of 150 μm internal diameter and the UVU resin, NEA 123T.

Figure 7b shows optical images of the microsprings fabricated at different deposition speeds (0.1–0.7 mm/s) and a constant extrusion pressure of 1 MPa. At a relative low deposition speed (0.1–0.2 mm/s) the extruded filament did not follow the designed path. For an accurate fabrication, the UV exposure zone should be adjusted such that the filament is exposed to the light shortly after extrusion which allows the increase in rigidity upon curing. Therefore, at low deposition speeds, it takes longer for the filament before reaching the exposure region (meeting the light), thus the filament may slump by its weight as a result of incomplete curing. In other words, the rigidity of the extruded filaments was not high enough (i.e.,  $E < E_c$ ) to provide structural support for the material being deposited. In addition to incomplete curing, the possible filament bending due to the

mismatch between the deposition speed (0.4 mm/s) and the extrusion pressure/speed contribute to some extent to the unsuccessful fabrication. As the deposition speed increased (0.3–0.4 mm/s), stable filaments with geometries close to the designed parts were observed. The best match was achieved at the deposition speed of 0.4 mm/s (matching the extrusion pressure/speed of 0.4 mm/s) that enabled the accurate fabrication of microsprings composed of seven turns for a height of 7 mm with the middle coils having a pitch of 1 mm. A further increase of the deposition speed (0.5–0.7 mm/s) led to the fabrication of the microcoils with a smaller diameter than their programmed diameter. This issue may come from the fact that the rigidity increase of newly deposited material is not high enough due to the short UV exposure time. Therefore, the extruded filament has the same rigidity from its extrusion point to the previous support point so that the filament starts moving the extrusion nozzle changing direction. To address this issue and have relatively high fabrication rates, materials with higher polymerization rates should be used. Another contribution may come from the mismatch between the deposition speed and the extrusion pressure/speed (> 0.4 mm/s) that leads to the stretching and the deformation of the filament.

### 3.2.3. Extrusion pressure

The effect of the extrusion pressure on the 3D printing of the structures was investigated, while keeping the deposition speed constant. Figure 8 shows optical images of the vertical lines fabricated at seven different extrusion pressures (0.5–35 MPa) and a constant deposition speed of ~0.5 mm/s. The extrusion speed of the material inside the micro nozzle was estimated for the seven extrusion pressures by extrapolating the apparent viscosity of the material (Figure 3) and using Equation 1 (see section 3.2.2). Table 1 lists the estimated extrusion speeds for the seven extrusion pressures used. The fabricated vertical filaments were straight and stable for the pressures up to 2 MPa with the increase of filaments' diameter with increasing the extrusion pressure. Above this pressure, either waved or non-shaped filaments were observed, confirming the importance of matching the extrusion pressure/speed and the deposition speed. As listed in Table 1, for the first two relatively low pressures (0.5–1 MPa), the estimated extrusion speeds were below the deposition speed (0.5 mm/s). Therefore, filament stretching is most possibly responsible for the smaller diameter of the filaments (< the extrusion nozzle's ID). The fabrication of the filaments at the pressures of 2 MPa and 3 MPa gradually made the filaments less stable and produced bending instability. This instability is possible because of insufficient UV exposure time, and also bending of filament as a result of the deposition speed and extrusion pressure/speed mismatch (0.5 mm/s) for the relatively high material flow rate.



Table 1. Estimated extrusion speeds based on capillary equations for seven extrusion pressures us

Extrusion pressure (MPa)	Extrapolated viscosity from Figure 3a (Pa.s)	Estimated extrusion speed based on capillary equations (mm/s)
0.5	240	0.1
1	115	0.4
1.5	100	0.6
2	80	1.2
2.5	70	1.6
3	65	2.3
3.5	60	2.9

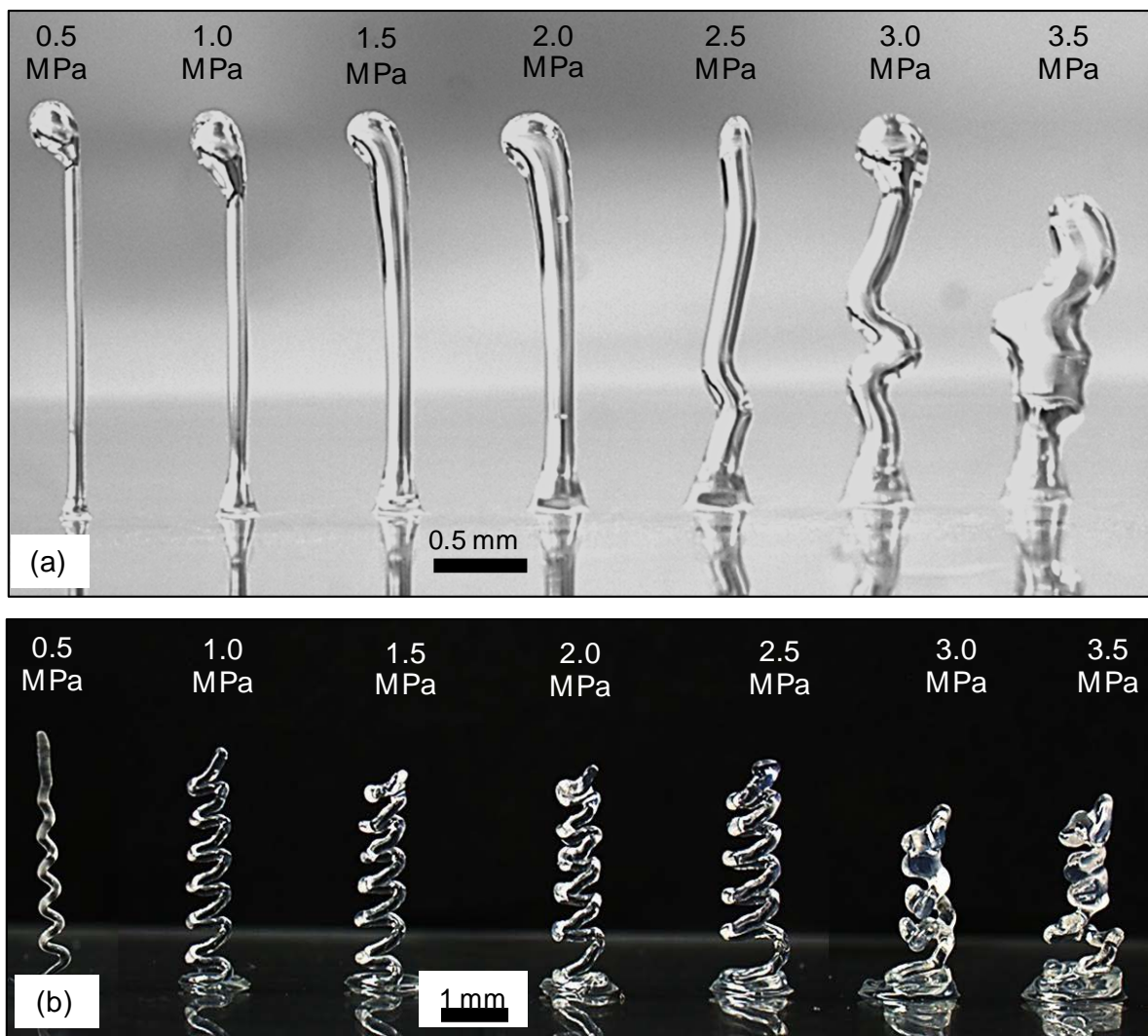


Figure 8. UV-3DP fabrication of (a) vertical filaments and (b) freeform microsprings at different extrusion pressures and a constant deposition speed of ~ 0.5 mm/s using an extrusion nozzle of 150  $\mu$ m internal diameter and the UVU resin, NEA 123T.

Figure 8b shows optical images of the microsprings fabricated at different extrusion pressures (0.5 – 3.5 MPa) while maintaining a constant deposition speed of 0.5 mm/s. The fabrication of microsprings at the lowest extrusion pressure (0.5 MPa) was unsuccessful as either the extruded



material lost their filamentary shape mostly after the first coil was fabricated or a vertical wavy filament was obtained, as can be seen in Figure 8b. This relatively low extrusion pressure (associated to an extrusion speed of 0.1 mm/s) may result in a mismatch with the deposition speed which leads to stretching of the filament when the deposition speed was set at 0.5 mm/s. At the pressures above 1 MPa, more stable filaments were observed, although the fabricated microsprings featured different shapes, heights and coil diameters. At pressures of 1 and 1.5 MPa, the estimated material extrusion speeds of 0.4 - 0.6 mm/s (see Table 1) were close to the deposition speed of 0.5 mm/s. Thus, the microsprings geometry were close to the programmed design, indicating the proper selection of the processing parameters. Similar to the microsprings fabricated at low deposition speeds (0.1 – 0.2 mm/s) shown in Figure 7b, applying relatively higher pressures (3.5 MPa) led to the fabrication of non-shape structures most probably due to incomplete curing of the filament and so their possible bending caused by a mismatch between the deposition speed and the extrusion pressure.

### 3.3. Processing map based on material and processing criteria

The experiments shown in section 3.2 were selectively repeated for a few materials either pure resins or their nanomaterials filled nanocomposites having shear thinning viscosity behavior similar to those shown in Figure 3. The extrusion nozzle diameter used were 100  $\mu\text{m}$  or 150  $\mu\text{m}$ . A processing map was created under those conditions for the UV-assisted 3D printing technique. Figure 9 shows the processing map drawn based on the two most important processing parameters which are the extrusion pressure and the deposition speed. The diameter of the extrusion nozzle is found to affect only the extrusion pressures so that less pressure is required for the extrusion of material through larger nozzle diameter and vice versa. The UV intensity was set for all the experiments 50 mW/cm<sup>2</sup>, match with the UV curing kinetics of the materials. The UV-exposure zone was also adjusted such that the filament is exposed to the UV radiation slightly after extrusion and kept constant.

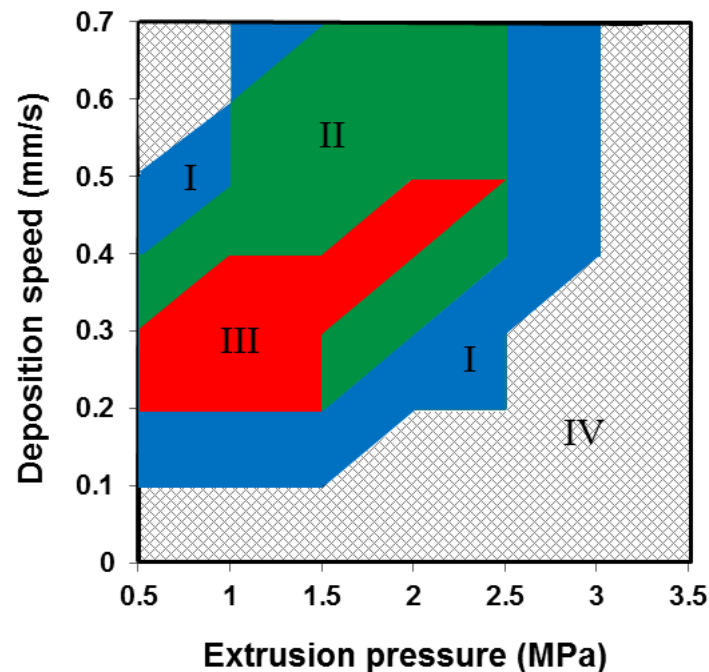


Figure 9. UV-3DP processing map for the fabrication of different microstructures at an adjusted U intensity and exposure zone. Zone I (blue): vertical microrods, Zone II (green): self-supported structures, Zone III (red): 3D freeform structures, and Zone IV: unsuccessful fabrication.

For successful and accurate fabrication of vertical microrods, 3D self-supported and 3D freeform microstructures, the manufacturing parameters as well as the intrinsic properties of the materials have to be properly chosen. After a material met the criteria for the viscosity and polymerization rate required for the 3DP technique, the extrusion pressure and the speed will be matched to achieve the critical conversion rate, which may vary depending on the desired geometry. The large area of zone I indicates that a vertical microrod can be fabricated in a broad range of pressures and speeds using different materials. Zone II which is part of Zone I, shows that the range of the parameters are limited for the fabrication of self-supported or layer-by-layer microstructures when compared to those of the microrods. It indicates that a higher value of  $\eta_c$  is required for the fabrication of layered structures due to possible buckling of the filaments between two supports at an incomplete curing. Processing zone is much narrower for the fabrication of 3D freeform structures as shown in Figure 9, Zone III. Further increase of the filament rigidity (i.e., much higher  $\eta_c$ ) is required, which limits the range of extrusion pressures and speed. In this study, a slight mismatch between the extrusion pressure and deposition speed affects the fabricated structure shapes which may be far from the programmed trajectory. Zone IV shows the range of parameters in which the UV 3DP was unsuccessful with our UV setup and the materials used in this study. In general, the fabrication of the 3D complex structures is found to be more complicated than that of vertical microrods in which the fabricated filament is along the direction of extrusion. This allows the vertical filament to uniformly expose to the UV light, which is not the case for the 3D self-supported and freeform microstructures.

### 3.4. Fabrication of 3D supported and freeform structures

Various complex freeform and self-supported microstructures were fabricated as shown in Figure 10. Table 2 lists the detailed information of the manufactured microstructures such as geometry, feature size, processing conditions and typical materials used. Figure 10a shows SEM image of a typical filament circular cross-section having a diameter of  $\sim 20 \mu\text{m}$ . The filament spanned two rectangular pads with a distance of 10 mm and was fabricated with the UV-epoxy nanocomposite (containing 1 wt.% CNTs). The fabricated very high aspect ratio (Length/Diameter (L/D) equals to  $\sim 65$ ) filament could be used as highly sensitive nanocomposite sensor to accurately measure the strain of a structure under mechanical loading. In general, the concept of nanocomposite-based strain sensors is based on their electromechanical sensitivity that stems from the rearrangement of percolating conducting pathways (e.g., nanotubes pathways) by an external mechanical disturbance [5]. The freestanding feature of the filament fabricated here may lead to avoid capturing of undesired parasitic perturbations (local cracks, plasticity, etc.) applications where overall measurements are sought [14].

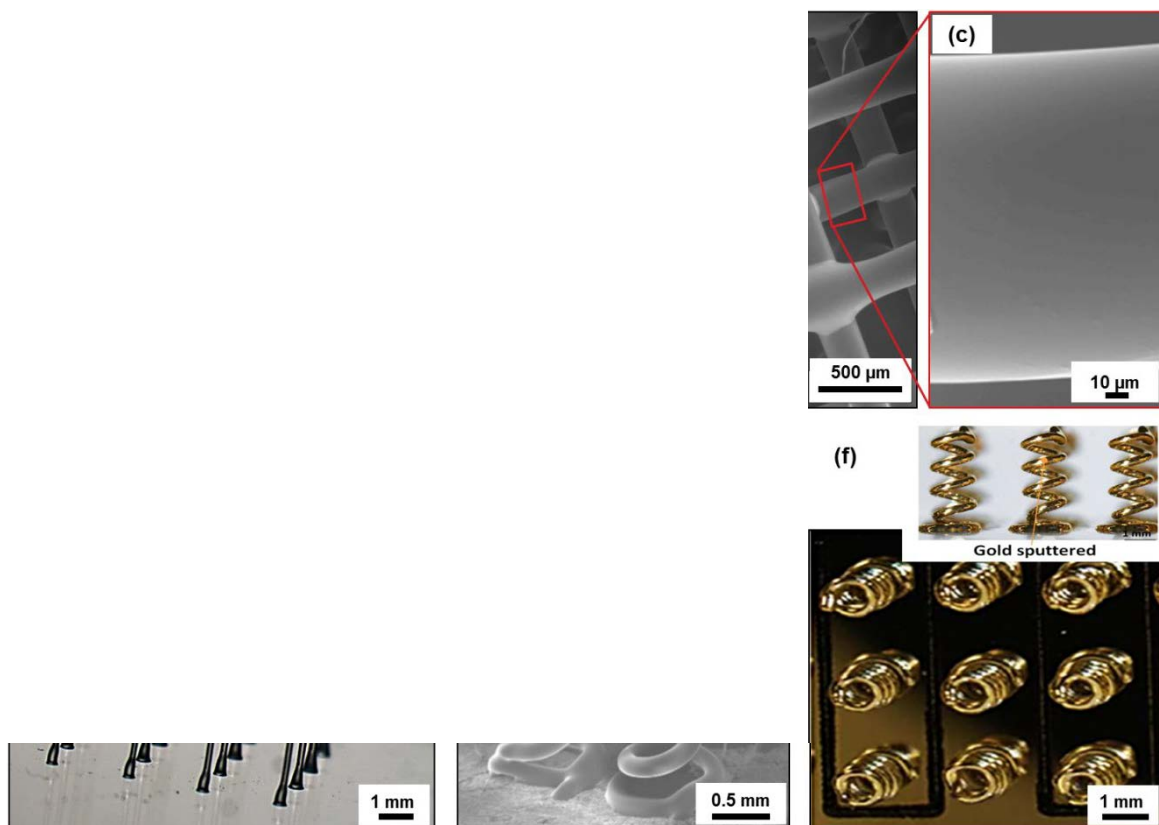


Figure 10. Optical and SEM images of several representative microstructures fabricated using the-UV 3DP technique: (a) typical fabricated filament cross-section, (b) a 3D periodic 4-layer scaffold, (c) higher magnification of (b), (d) a network of 16 vertical microrods, (e) a network of 4 nanocomposite microspheres, (f) a network of gold-sputtered microspheres electrodes

Table 2. Detailed information (geometry, feature size, processing conditions and materials) for the fabrication of microstructures shown in Figure 10.

Fig. 10	Geometry and feature size	Materials used	Nozzle ID ( $\mu\text{m}$ )	Extrusion pressure (MPa)	Deposition speed (mm/s)
(a)	A single filament having 10 mm length	UV-epoxy nanocomposites (1wt.% CNTs)	100	$\sim 1.5$	0.4
(b, c)	4-layers scaffold with filament span of 1 mm	UV-PU (NEA 123T)	150	$\sim 1.5$	0.3
(d)	A network of 16 vertical rods (L/D:100)	UV-PU (NEA 123T)	150	$\sim 1$	0.6
(e)	A network of 4 microsprings	UV-epoxy nanocomposites (1wt.% CNTs)	100	$\sim 1.5$	0.2
(f, g)	A network of 15 gold sputtered microsprings	UV-PU (NEA 123T)	150	$\sim 1$	0.4

The flexibility of the UV3DP methods enabled to fabricate 3D periodic scaffolds with a desired overall size, filaments length and diameter having potential applications in tissue engineering. In these applications, filament spacing (or porosity of the structure) is of importance. Figure 10b displays the enlarged SEM image of a representative scaffold featuring 15 filaments in each layer in a square fashion, which composed of the filaments having a length of  $\sim 15$  mm and diameter of  $\sim 200\mu\text{m}$  with the filament spacing of 1 mm. Figure 10c is a close view of the smooth surface of a filament in Figure 10b. Contrary to other techniques such as printing of a fugitive ink filaments whose spacing in a given layer is limited to approximately times the filament diameter (L/D of 10) [16], the significant increase of the filament rigidity in the 3DP technique prevents sagging of the filaments fabricated over the underlying layer featuring a long filament spacing. Owing to this unique capability, the spacing between filaments (i.e., structural porosity) given layer could be easily tailored in order to provide an appropriate condition, in term of structural parameters, for cell attachment and growth [7].

Figure 10d shows optical image of a microrods network composed of 16 identical microrods having a length of  $\sim 15$  mm and a diameter of  $\sim 150\mu\text{m}$  (L/D of  $\sim 100$ ). The network was fabricated in a square layout (44) having a rod spacing of 3 mm. This type of microdevice might find applications in MEMS and lab-on-a-chip systems, for instance, as surface enhancement textures in gas and biosensors and solar cells [18]. In the literature, a rod aspect ratio of up to 50 has been achieved using photolithography techniques in order to make such a device to entrap kidney cells on a network consisting of hundreds of microrods featuring considerably larger aspect ratio of up to few hundreds can be manufactured using the 3DP technique.

Figure 10e shows SEM image of network of microsprings made of carbon nanotube based nanocomposite materials with potential MEMS application such as free strain sensor with a possible capability of sensing out-plane strains [15]. This nanocomposite based microdevice

consists of four identical freeform microsprings with seven 1 mm diameter coils and intercoil distance of 3 mm. The height of microsprings was ~ 6 mm and the filament's diameter was ~ 150  $\mu\text{m}$ . Figure 10f shows optical image of a fabricated network which is composed of gold-sputtered 3D freeform microsprings with high potential in lab-on-a-chips. This manufactured interdigitated 3D microelectrode might be used to build a real lab-on-a-chip device in order to promote cell separation (e.g., cancer cell detection) through dielectrophoretic forces, representing higher efficiency when compared to standard planar microelectrodes [49]. The flexibility of the UV3DP technique enables the accurate fabrication of complex 3D microstructures with different geometries for various technological applications such as MEMS, microelectronics, and tissue engineering.

#### 4. Conclusion

In the present work, the effects of manufacturing conditions of the 3DP technique were thoroughly investigated in order to find a processing map for successful and accurate freeform fabrication of 3D self-supported and freeform structures. It was found that for successful and accurate fabrication of 3D structures, the deposition speed, the pressure applied to the material, and the UV radiation intensity have to be adjusted according to the viscosity and the curing rate of the extruded material. Once the proper condition was applied, the manufactured microstructures geometry matched the programmed robot's paths and the fabrications were reproducible. A higher increase of the filament rigidity was required for the fabrication of freeform microstructures, which limited the processing condition to a much narrower zone, when compared to that of supported structures. The detailed results presented in this study may help understand better the parameters influencing the UV3D printing of microstructures with various geometries and may offer a general overview of the technique with its capabilities. Further studies should focus on the creation of a dimensionless processing map to extend its applicability. This next step will require taking into account the materials photopolymerization kinetics during the fabrication of a structure.

#### 5. Acknowledgements

The authors acknowledge the financial support from FQRNT (Le Fonds Québécois de la Recherche sur la Nature et les Technologies). The authors would like to thank the technical advice from Professor Martin Levesque from Ecole Polytechnique de Montréal.

#### 6. References

- [1] Thostenson E T and Chou W W 2006 Carbon nanotube networks: Sensing of distributed strain and damage for life prediction and self healing Adv. Mater. 18 2837-41
- [2] Sandler J K W, Kirk J E, Kinloch I A, Shaffer M S P and Windle A H 2003 A low electrical percolation threshold in carbon nanotube epoxy composites Polymer 44 5893-9

- [3] Tsai Y C, Li S C and Chen J M 2005 Electrochemical Sensors Based on Multi Carbon Nanotube/Nafion<sup>TM</sup> Nanocomposite Film for Determination of Heavy Metals and Hydrogen Peroxide Proceedings of 2005 5th IEEE Conference on Nanotechnology, Nagoya, Japan
- [4] Sahoo N G, Jung Y C, Yoo H J and Cho J W 2007 Influence of carbon nanotube and polypyrrole on the thermal, mechanical and electroactive properties of polyurethane nanocomposites Compos. Sci. Technol. 67 1920-9
- [5] Halary J, Cookson P, Stanford J L, Lovell P and Young R J 2004 Smart nanostructured polymeric coating for use as remote optical strain sensor Advanced Engineering Materials 6 729
- [6] Liska R, Schuster M, Infuhr R, Turecek C, Fritscher C, Seidl B, Schmidt V, Kuna L, Haase A, Varga F, Lichtenegger H and Stampf J 2007 J. Coat. Technol. Res. 4 505
- [7] Kawata S, Sun H B, Tanaka T and Takada K 2001 Finer features for functional microdevices Nature 412, 6848
- [8] Lebel L L, Aissa B, El Khakani M A and Therriault D 2010 Ultraviolet assisted direct write fabrication of carbon nanotube/polymer nanocomposite microfluidic devices Mater. 22 592
- [9] Le Borgne V, Aissa B, Mohamedi M, Kim Y A, Endo M, El Khakani M A 2011 Single wall laser synthesis of single wall carbon nanotubes: effects of catalyst content and furnace temperature on their nanostructure and photoluminescence properties Journal of Nanoparticle Research 13 5759
- [10] Farahani R D, Dalir H, Le Borgne V, Gautier L A, El Khakani M A, Lévesque M and Therriault D 2012 Reinforcing epoxy nanocomposites with functionalized carbon nanotubes via biotin streptavidin interaction Compos. Sci. Technol. 72 12
- [11] Zein I, Huttmacher D W, Tan K C and Teoh S H 2002 Fabrication and composition modeling of novel scaffold architectures for tissue engineering applications Biomaterials 23 1169
- [12] Bruneaux J, Therriault D, Heuzey MC 2008 Microextrusion of organic inks for direct write assembly Journal of Micromechanics and Microengineering 18 1-8
- [13] Lebel L L, Aissa B, El Khakani M A and Therriault D 2010 Preparation and mechanical characterization of laser ablated single walled carbon nanotubes/polyurethane nanocomposite microbeams Compos. Sci. Technol. 70 3
- [14] Farahani R D, Dalir H, Le Borgne V, Gautier L A, El Khakani M A, Lévesque M and Therriault D 2012 Direct write fabrication of freestanding nanocomposite strain sensors Nanotechnology 23 238
- [15] Hu N, Karube Y, Yan C, Masuda Z and Fukunaga H 2008 Tunneling effect in a polymer nanotube nanocomposite strain sensor Acta Materialia 56 13
- [16] Therriault D, White S R and Lewis J A 2003 Chaotic mixing in three dimensional microvascular networks fabricated by direct write assembly Nature Mater 2 265
- [17] Kan Wang L C, Zhang L, Dong J and Wang S 2012 Biodegradable-phospholinked polymer substrates with concentric microgrooves for regulating MCF-7 cell behavior Adv. Healthc. Mater. 1 10
- [18] Yoo J S, Kim K, Thamilselvan M, Lakshminarayn N, Kink Y and Lee J 2008 RIE texturing optimization for thin c-Si solar cells in SF<sub>6</sub>/O<sub>2</sub> plasma Appl. Phys. Lett. 91 125205
- [19] Khoshmanesh K, Zhang C, Tovar F J, Nahavandi S, Baratchi S, Mitchell A and Kalantar Zadeh K 2010 Dielectrophoretically activated cell sorting based on curved microelectrodes Microfluid. Nanofluid. 14 411